

## Elastic and Inelastic Scattering of 20.3-MeV Polarized Protons from $^{90}\text{Zr}$ , $^{92}\text{Zr}$ , and $^{92}\text{Mo}$ †

C. GLASHAUSSER AND R. DE SWINIARSKI,\*

*Service de Physique Nucléaire à Moyenne Energie, Centre d'Etudes Nucléaires, Saclay, France and Lawrence Radiation Laboratory, University of California, Berkeley, California 94720*

AND

J. GOUDERGUES, R. M. LOMBARD,‡ B. MAYER, AND J. THIRION

*Service de Physique Nucléaire à Moyenne Energie, Centre d'Etudes Nucléaires, Saclay, France*

(Received 14 March 1969)

The elastic and inelastic scattering of polarized protons from  $^{90}\text{Zr}$ ,  $^{92}\text{Zr}$ , and  $^{92}\text{Mo}$  has been studied at 20.3 MeV. Asymmetries for the first  $2^+$  states in  $^{90}\text{Zr}$  and  $^{92}\text{Mo}$  are very similar; the  $^{92}\text{Zr}$   $2^+$  asymmetry is quite different from these, especially at large angles. The asymmetry for the first  $3^-$  state in  $^{92}\text{Zr}$  resembles the  $^{90}\text{Zr}$ - $^{92}\text{Mo}$   $3^-$  data more closely. Microscopic-model calculations for the  $2^+$  states with and without core-polarization contributions give poor fits to the asymmetry data, though cross sections are well fitted. Macroscopic-model calculations with the full Thomas form of the deformed spin-orbit potential give a better fit to the  $2^+$  data and quite closely predict the  $3^-$  asymmetries.

### I. INTRODUCTION

RECENT attempts to interpret asymmetries in the inelastic scattering of polarized protons have been only partially successful.<sup>1-3</sup> The predictions of the distorted-wave Born-approximation (DWBA) or coupled-channels methods were reasonably accurate for  $2^+$  and  $3^-$  states in  $^{56}\text{Fe}$  and the nickel isotopes at energies between 18.6 and 40 MeV. A macroscopic description was used; the good results were obtained only by including real, imaginary, and spin-orbit terms in the form factors. This model was unable, however, to reproduce the large asymmetries observed after excitation of the first  $2^+$  state in  $^{52}\text{Cr}$  and  $^{54}\text{Fe}$  which have 28 neutrons. (The differences between  $^{54}\text{Fe}$  and  $^{56}\text{Fe}$  have recently been verified at 19.6 MeV.<sup>4</sup>) The fact that neighboring nuclei exhibited such large differences in asymmetries suggested that a microscopic analysis was necessary. However, on the assumption of simple configurations for the states involved, the microscopic form factors closely resembled the real central part of the macroscopic form factors; neither the cross sections nor the asymmetries were well fitted.

Some of the problems in the microscopic analysis may have arisen from the neglect of collective cor-

relations in the wave functions. Love and Satchler<sup>5</sup> have recently shown that core polarization (CP) can account for a large part of the cross section to states which are predominantly simple configurations. In their phenomenological model, a macroscopic-type form factor is added to the direct (D) microscopic form factor; its strength is proportional to the effective charge determined from electromagnetic decay rates. The model has been successfully applied in the analysis of differential cross sections for the excitation of  $2^+$  and  $4^+$  states in  $^{90}\text{Zr}$  and  $^{92}\text{Zr}$  at several energies, but it has not yet been used in the analysis of asymmetry data. Since the CP amplitude contains both imaginary and spin-orbit terms and is coherent with the D amplitude, it could produce large changes in the predicted asymmetries.

The  $2^+$  state in  $^{90}\text{Zr}$  at 2.18 MeV is excited predominantly by a proton transition of the type  $(1g_{9/2})_0^{-2} - (1g_{9/2})_2^{+2}$ , since the neutron shell is closed. The first  $2^+$  state in  $^{92}\text{Mo}$  at 1.51 MeV is also expected to be simply described in terms of  $1g_{9/2}$  protons. However, the  $2^+$  state in  $^{92}\text{Zr}$  is chiefly a  $(2d_{5/2})^2$  neutron configuration. The  $3^-$  state in each nucleus is strongly collective.

The macroscopic model would predict similar shapes for the differential cross sections and asymmetries for the  $2^+$  states and for the  $3^-$  states in all these nuclei. On the other hand, in the microscopic model without core polarization, variations between  $^{92}\text{Zr}$  and  $^{90}\text{Zr}$ - $^{92}\text{Mo}$  could arise from differences in the  $p$ - $p$  and  $p$ - $n$  effective interactions, and from differences in the form factors for transitions of  $2d_{5/2}$  and  $1g_{9/2}$  nucleons. When core polarization is included these effects are decreased, since both proton and neutron core excitations of similar types are likely to occur in all

† Work supported in part by the U. S. Atomic Energy Commission.

\* NATO Fellow. Permanent address: Institut des Sciences Nucléaires, Grenoble, France.

‡ Present address: Laboratoire de Physique Atomique et Moléculaire, Collège de France, Paris, France.

<sup>1</sup> C. Glashauser, R. de Swiniarski, J. Thirion, and A. D. Hill, *Phys. Rev.* **164**, 1437 (1967).

<sup>2</sup> M. P. Fricke, E. E. Gross, and A. Zucker, *Phys. Rev.* **163**, 1153 (1967); V. E. Lewis, M. Calderbank, N. K. Ganguly, and M. P. Fricke, *Nucl. Phys.* **A117**, 673 (1968).

<sup>3</sup> C. Glashauser and J. Thirion, in *Advances in Nuclear Physics*, edited by M. Baranger and E. Vogt (Plenum Press, Inc., New York, 1969), Vol. II, p. 79.

<sup>4</sup> B. Mayer and J. Thirion (private communication).

<sup>5</sup> W. G. Lovar and G. R. Satchler, *Nucl. Phys.* **A101**, 424 (1967).

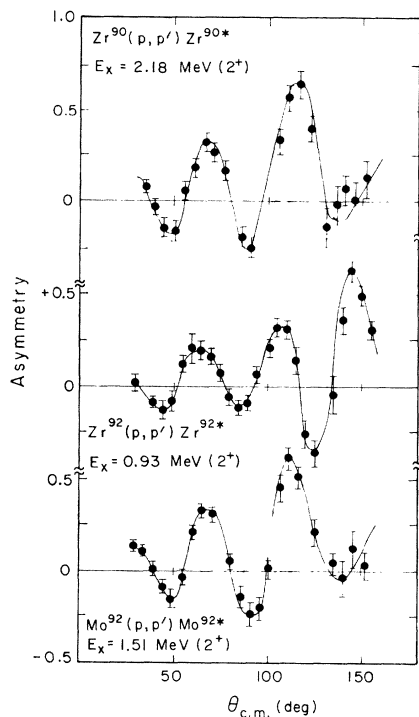


FIG. 1. Measured asymmetries, normalized to 100% beam polarization, as a function of c.m. scattering angle. The error bars are relative; the lines are visual guides.

three nuclei. However, the interference of the core-polarization amplitudes with the direct amplitudes can also produce experimental differences between  $^{90}\text{Zr}$ - $^{92}\text{Mo}$  and  $^{92}\text{Zr}$ . Differences between  $^{90}\text{Zr}$  and  $^{92}\text{Mo}$  would be expected to be small according to all these models.

After a discussion of the experimental methods in Sec. II, experimental differential cross sections and asymmetries for elastic scattering and inelastic scattering to the first  $2^+$  and  $3^-$  states in the three nuclei will be presented in Sec. III. The determination of optical parameters is described in Sec. IV A; in Sec. IV B, microscopic and macroscopic analyses of the inelastic data are presented. Section V includes a short summary and conclusions.

## II. EXPERIMENTAL METHOD

All data were taken with the proton beam at the Saclay sector-focused cyclotron; the energy was  $20.25 \pm 0.10$  MeV. The polarized ion source for this machine has been previously described; it utilizes the adiabatic transition method.<sup>6</sup> The neutral polarized beam is now ionized outside the cyclotron in an ionizer of new design.<sup>7</sup> The protons are then injected into the center of the cyclotron along the median plane.<sup>8</sup> They follow

<sup>6</sup> A. Abragam and J. M. Winter, Phys. Rev. Letters **1**, 375 (1958).

<sup>7</sup> P. Birien *et al.* (unpublished).

<sup>8</sup> R. Beurtey and J. M. Durand, Nucl. Instr. Methods **57**, 313 (1967).

a trochoidal path achieved by balancing the vertical magnetic field with a horizontal electric field produced by maintaining appropriate voltages on a set of copper bars along the injection path. Extracted beams were generally 10–30 nA, with a polarization of 70–80%. The sign of the polarization was reversed every 0.2 sec.

The deflected beam passes through a switching magnet and an achromatic system of two  $45^\circ$  bending magnets to a scattering chamber. The beam spot on the target was about  $2 \times 6$  mm<sup>2</sup>; with the detectors set 75 mm away, the angular resolution was  $\pm 2^\circ$ . A set of eight detector telescopes, each  $10^\circ$  apart, were mounted on two movable arms on both sides of the beam line; the possible angular range was  $20^\circ$ – $115^\circ$  on the right and  $70^\circ$ – $165^\circ$  on the left. (Note that because of the rapid reversal of the sign of the polarization, it was not necessary to repeat the same angle on both sides.) Generally, 10–12 Si(Li) detectors were actually mounted during a run, and the best eight of these were used in collecting data. All were cooled by Freon to about  $-25^\circ\text{C}$ . The energy resolution varied between 100 and 150 keV, of which about 50 keV could be attributed to beam spread.

The electronics were developed here to handle simultaneously 16  $\Delta E$ - $E$  telescopes, two beam intensity monitors and a polarimeter. Thus, a total of 40 pre-amplifiers were connected directly to vacuum feed throughs on two sides of the 45-cm hexagonal chamber. (Although no particle identification was performed during the present experiment,  $\Delta E$  detectors were sometimes used to aid in the parallel development of such a system.) The  $E$  and  $\Delta E$  pulses were summed

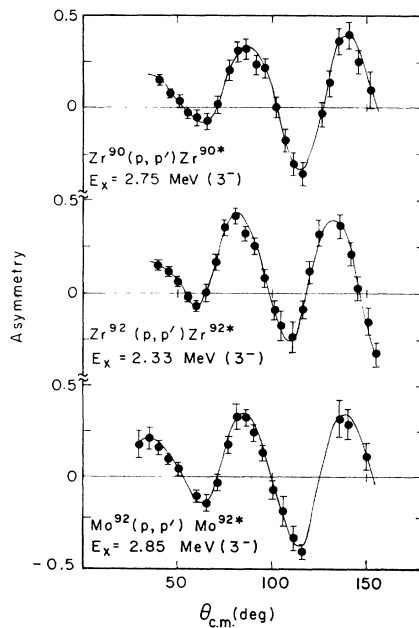


FIG. 2. Measured asymmetries for  $3^-$  states. The lines are visual guides.

at the input of an amplifier gated by a discriminator on the  $E$  preamplifier. The outputs of all the  $(E+\Delta E)$  amplifiers were mixed and fed into one biased amplifier, and then into an Intertechnique 4096-channel pulse-height analyzer. The  $E$  discriminator output served as a routing signal; a second routing signal was derived from the clock circuit controlling the two spin states of the beam. Since only eight telescopes were actually used during a run, 16 spectra of 256 channels each were recorded at the same time. Data were read out of the analyzer on paper tape and analyzed by hand or with peak-fitting programs when necessary.

Two detectors placed at  $40^\circ$  above and below the beam served as monitors of beam intensity. The outputs of discriminators adjusted to pass the elastic counts from these detectors were counted both in ungated scalers and in scalers gated on only during the live time of the analyzer. The difference in the two results was a measure of the dead time of the analyzer. When this exceeded about 10%, the elastic peaks in the most forward detectors were gated out of the spectra before the analyzer. The elastic data for these angles were then taken separately at lower beam currents. Differences in dead time associated with the two spin states were also monitored from time to time, but these were never significant.

The polarization of the beam was continuously monitored with a carbon polarimeter modeled after the Harwell polarimeter<sup>9</sup> whose absolute efficiency has been measured. Since the geometry and the carbon target thickness had to be modified to lower the counting rate in the detectors to a reasonable value,

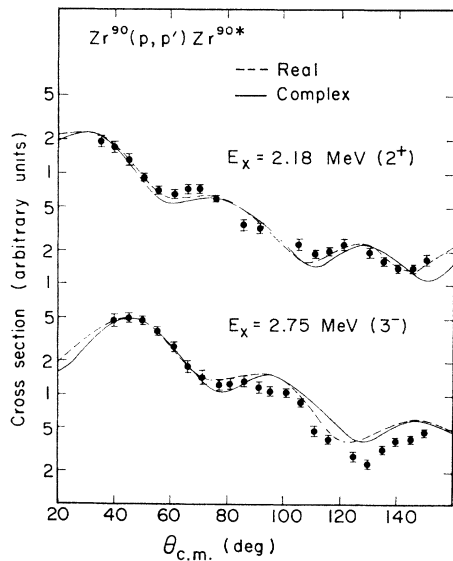


FIG. 3. Relative cross sections for  $^{90}\text{Zr}$ . The curves are macroscopic-model predictions described in the text.

<sup>9</sup> R. M. Craig, J. C. Dore, G. W. Greenlees, J. S. Lilley, J. Lowe, and P. C. Rowe, Nucl. Instr. Methods **30**, 269 (1964).

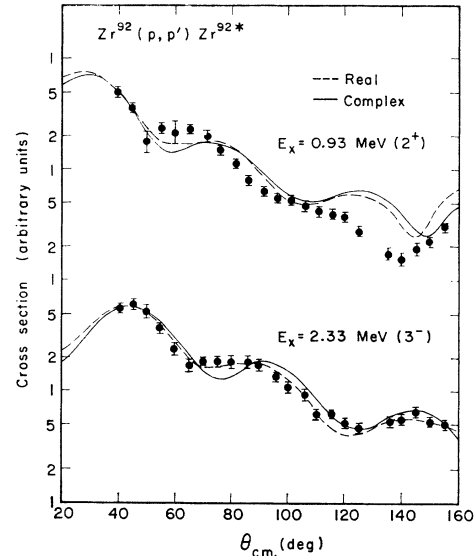


FIG. 4. Relative cross sections for  $^{92}\text{Zr}$ . The curves are macroscopic-model predictions described in the text.

some recalibration was necessary. The beam polarization measured with this polarimeter was compared with that measured with a  $^4\text{He}$  polarimeter on an adjacent beam line. The value of the efficiency was thus adjusted from the 0.57 of the Harwell polarimeter to  $0.55 \pm 0.03$ .

The targets were all about  $1 \text{ mg/cm}^2$  thick; they were obtained from ORNL. The purities of the  $^{90}\text{Zr}$ ,  $^{92}\text{Zr}$ , and  $^{92}\text{Mo}$  targets were 98.0, 93.2, and 97.6% respectively.

### III. RESULTS

Asymmetry data for the first  $2^+$  and  $3^-$  states in these nuclei are shown in Figs. 1 and 2. The asymmetry is normalized to 100% beam polarization, and is defined as follows:

$$A = (1/P_B)(N_+ - N_-)/(N_+ + N_-).$$

The quantity  $P_B$  is the measured polarization of the beam;  $N_+$  and  $N_-$  are the counts in a given peak for incoming protons with spin up and spin down, respectively. The Basel sign convention is followed.

The errors shown are generally purely statistical, unless there was difficulty in peak separation. The latter contributes significantly only to the error in the  $^{90}\text{Zr}$   $2^+$  data, since a  $5^-$  state lies 130 keV away. Two independent peak-fitting programs used to extract the data for this peak gave consistent results. As a check on possible systematic errors from one run to the next, data for  $^{12}\text{C}$  and  $^{16}\text{O}$  were repeated frequently, with consistent results. The carbon data agree only qualitatively, however, with those reported by Craig *et al.*<sup>10</sup> at the same energy; the discrepancies

<sup>10</sup> R. M. Craig, J. C. Dore, G. W. Greenlees, J. Lowe, and D. L. Watson, Nucl. Phys. **79**, 177 (1966).

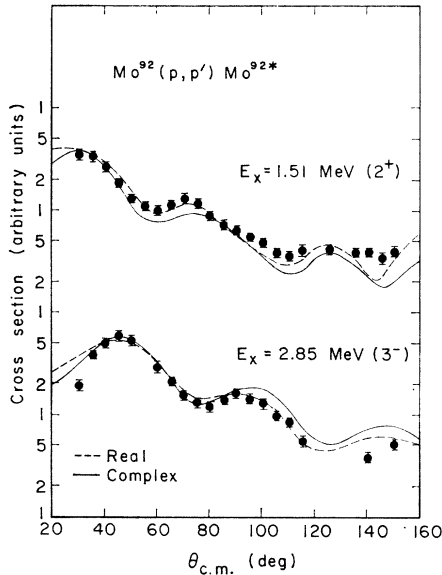


FIG. 5. Relative cross sections for  $^{92}\text{Mo}$ . The curves are macroscopic-model predictions described in the text.

cannot be explained by an error in the absolute normalization of the polarization but may be due to resonance structure. The data for  $^{16}\text{O}$  agree well with that reported by Boschitz *et al.* at 20.7 MeV.<sup>11</sup> However, Lowe *et al.*<sup>12</sup> have recently suggested there is a resonance in  $p+^{16}\text{O}$  scattering at 20.3 MeV. Polarization data obtained for elastic scattering from  $^{40}\text{Ca}$  in this same series of experiments is consistent with data recently obtained at Berkeley at the same energy.<sup>13</sup>

Cross sections are shown in Figs. 3–5, together with theoretical curves described below. Errors of  $\pm 10\%$  have generally been assigned. This is larger than the statistical error, but it is a conservative estimate of the reproducibility of the data points at angles where cross sections were measured by several counters. (These errors arise primarily from differences in solid angle and detector efficiencies and did not affect the polarization measurements.) It was not convenient to obtain absolute cross sections since no Faraday cup was used. They have been measured previously for  $^{90}\text{Zr}$  and  $^{92}\text{Zr}$  at nearby energies.<sup>14,15</sup>

The most interesting feature of the data in Figs. 1–5 is the remarkable similarity in the results for  $^{90}\text{Zr}$

<sup>11</sup> E. T. Boschitz, M. Chabre, H. E. Conzett, and R. J. Slobodrian, in *Proceedings of the Second International Symposium on Polarization Phenomena of Nucleons, Karlsruhe, 1965*, edited by P. Huber and H. Schopper (Birkhauser Verlag, Basel, Switzerland, 1966), p. 331.

<sup>12</sup> J. Lowe (private communication).

<sup>13</sup> R. de Swiniarski, A. D. Bacher, J. Ernst, A. Luccio, F. Resmini, R. Slobodrian, and B. Tivol, *Bull. Am. Phys. Soc.* **13**, 1663 (1968).

<sup>14</sup> W. S. Gray, R. A. Kenefick, J. J. Kraushaar, and G. R. Satchler, *Phys. Rev.* **142**, 735 (1966).

<sup>15</sup> M. M. Stautberg and J. J. Kraushaar, *Phys. Rev.* **151**, 969 (1966).

and  $^{92}\text{Mo}$  compared with those for  $^{92}\text{Zr}$ . This is most noticeable in the  $2^+$  asymmetry data. The  $^{90}\text{Zr}$  and  $^{92}\text{Mo}$  curves overlap almost exactly within the errors, while the  $^{92}\text{Zr}$  curve goes out of phase at larger angles and includes an extra maximum at  $140^\circ$ . At the  $70^\circ$  maximum, the  $^{92}\text{Zr}$  asymmetry is also somewhat smaller than that for  $^{90}\text{Zr}$  and  $^{92}\text{Mo}$ . This corresponds to the peak for which large differences were observed between  $^{54}\text{Fe}$  and  $^{56}\text{Fe}$  at 18.6 MeV (and 19.6 MeV<sup>4</sup>); for both the  $A \sim 60$  and  $A \sim 90$  nuclei, it is the predominantly neutron excitations which yield smaller asymmetries than the predominantly proton excitations. The differences in differential cross sections between  $^{54}\text{Fe}$  and  $^{56}\text{Fe}$  noted earlier are also mirrored here. The relative cross section for  $^{92}\text{Zr}$  is considerably smaller than that for  $^{90}\text{Zr}$ – $^{92}\text{Mo}$  at large angles if the curves are normalized at  $40^\circ$ , just as the large-angle cross section for  $^{56}\text{Fe}$  is relatively smaller than that for  $^{54}\text{Fe}$ . Differences in the shapes of the  $2^+$  cross sections for  $^{90}\text{Zr}$  and  $^{92}\text{Zr}$  have been found earlier at several energies.<sup>14–16</sup>

Variations between  $^{90}\text{Zr}$ – $^{92}\text{Mo}$  and  $^{92}\text{Zr}$  are seen in the data for even the collective  $3^-$  states. The  $^{92}\text{Zr}$  asymmetry is about  $8^\circ$  out of phase with  $^{90}\text{Zr}$  at the last maximum, while the  $^{92}\text{Mo}$  asymmetry is in good agreement with  $^{90}\text{Zr}$ . There are also small differences in the shapes of the cross sections at both forward

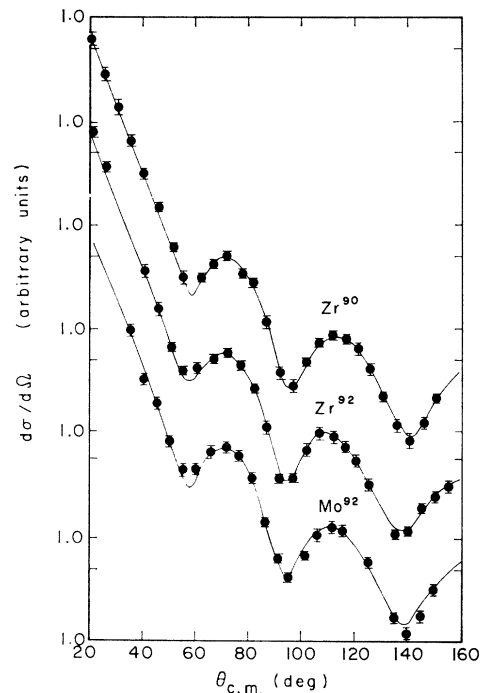


FIG. 6. Elastic-scattering cross sections and optical-model predictions with the parameters of Table I. The normalization was a free parameter.

<sup>16</sup> J. K. Dickens, E. E. Eichler, and G. R. Satchler, *Phys. Rev.* **168**, 1355 (1968).

and backward angles; these have been noted also at 12.7 MeV.<sup>16</sup> Since the  $4^-$  state in  $^{90}\text{Zr}$  is almost degenerate with the  $3^-$  state, it might account for some of the large angle differences although it is unlikely to be significant at small angles. The fact that the  $3^-$  data for  $^{92}\text{Mo}$  and  $^{90}\text{Zr}$  are very similar also indicates that the contribution of the  $4^-$  state in  $^{90}\text{Zr}$  is not important.

#### IV. ANALYSIS

##### A. Optical-Model Parameters

The optical-model parameters were determined from an analysis of the elastic cross-section and polarization data taken concurrently with the inelastic data described above. The search code MERCY, a modified version of SEEK,<sup>17</sup> was used. The definition of the optical potential and the search procedures employed are standard.<sup>1</sup> Errors on the cross sections were uniformly set at  $\pm 10\%$ ; the errors on the polarization were statistical unless these were very small. Corrections arising from the finite angular acceptance of the detectors were not included.

Good fits to the 18.6-MeV elastic scattering data for nuclei with  $A \sim 60$  have been obtained<sup>18</sup> by adopting several sets of fixed geometrical parameters for the central potential. The parameters of Perey ( $r_s = r_I = 1.25$  F,  $a_s = 0.65$  F,  $a_{s0} = a_I = 0.47$  F) and those of Satchler ( $r_s = 1.24$  F,  $r_I = 1.28$  F,  $a_s = 0.65$  F,  $a_I = 0.50$  F,  $a_{s0} = 0.42$  F) were about equally successful, although the latter gave better fits to the inelastic data. The spin-orbit radius  $r_{s0}$  found with both sets was generally about 10% less than the real radius  $r_s$ .

These parameters were tried for the present data, but only the second set gave reasonable agreement. The average value of  $r_{s0}$  was again about 10% less than  $r_s$ ; the values of  $\chi^2/N$  ranged from 5 to 7. Very good fits were finally obtained by searching on all parameters at once, starting from the best "Perey" and the best "Satchler" sets and several others. All initial values gave the same final results; these are listed in Figs. 6 and 7. Note that the best-fit parameters for the three nuclei are quite similar. The largest variations are observed in the value of  $r_{s0}$ , but the average value is again smaller than  $r_s$  by almost 15%. The improvement in the fit with the best-fit parameters is due chiefly to the increase in  $a_I$ . This was found to be true also in the analysis of 18.8-MeV cross-section results by Gray *et al.*<sup>14</sup>

Attempts were made to improve these fits by introducing some volume absorption, and also by including an imaginary spin-orbit term. As expected,

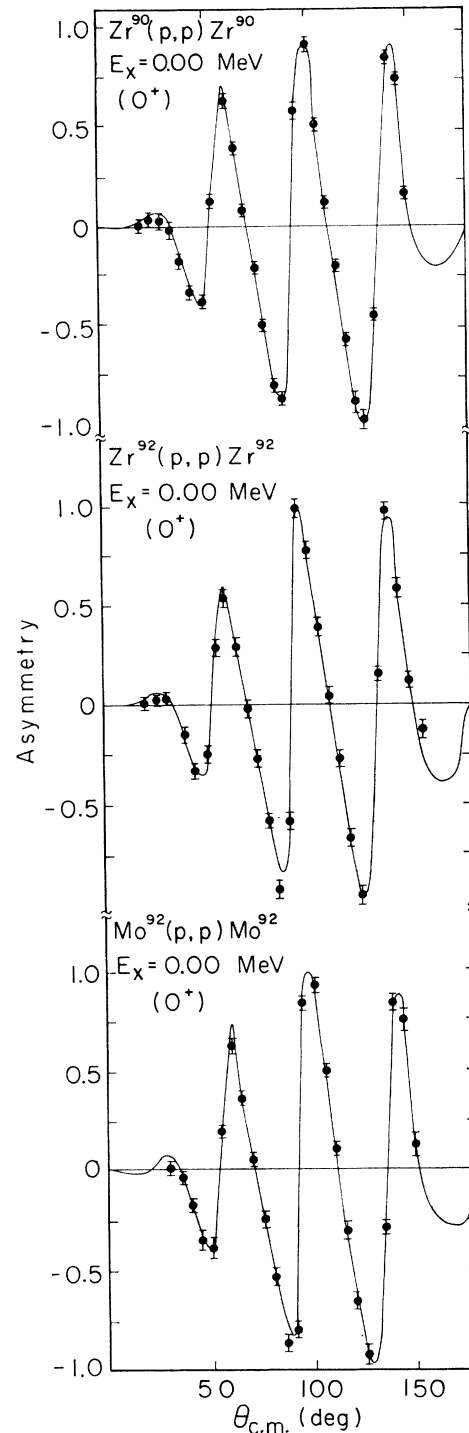


FIG. 7. Elastic-scattering asymmetries and optical-model predictions with the parameters of Table I.

<sup>17</sup> M. A. Melkanoff, J. Raynal, and T. Sawada, University of California at Los Angeles Report No. UCLA 66-10, 1966 (unpublished).

<sup>18</sup> P. Kossanyi-Demay, R. de Swiniarski, and C. Glashauser, Nucl. Phys. A94, 513 (1967); P. Kossanyi-Demay and R. de Swiniarski, *ibid.* A108, 577 (1968).

an increase in volume absorption reduced the surface absorption by an equivalent amount, but the quality of the fit rapidly deteriorated. On the other hand, fits almost as good as those of Figs. 6 and 7 could be obtained with an imaginary spin-orbit term of  $-1-$

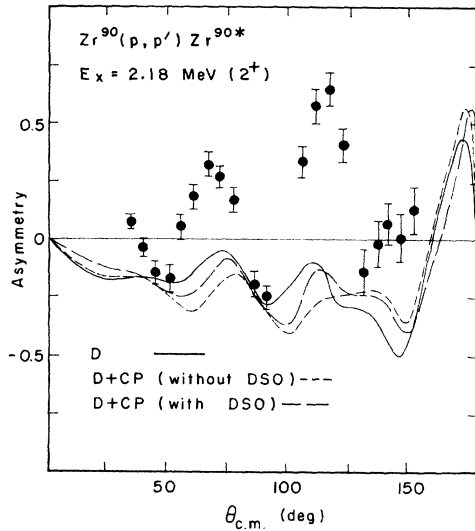


FIG. 8. Microscopic-model predictions for the 2.18-MeV state in  $^{90}\text{Zr}$ . The curves were computed with a direct term only (D), and with both direct- and core-polarization terms (D+CP). In the latter, the DSO term was included or neglected.

MeV strength after small adjustments of the other parameters. The best-fit value of  $W_{so}$  was still very close to zero, however.

### B. Reaction Models

The inelastic data have been analyzed with the Oxford coupled-channels program,<sup>19</sup> using both macroscopic and microscopic models.

#### 1. Microscopic Model

This model has been described in detail by several authors.<sup>20</sup> The incoming projectile is assumed to interact with the valence nucleons of the target; the potential is of the form

$$V_{ij}(r) = -(V_0 + V_1 \delta_{i \cdot} \delta_j) g(|r_{ij}|). \quad (1)$$

In the present work,  $g(|r_{ij}|)$  was taken as a Yukawa well of range 1 F. Contributions of spin transfer  $S=1$  were not included (i.e.,  $V_1$  was set to zero). Asymmetries predicted with  $S=1$  have previously been shown<sup>1</sup> to be very similar to  $S=0$  asymmetries for simple configurations, and the interference between  $S=0$  and  $S=1$  is small. Nucleon-nucleon tensor and spin-orbit forces should also be included in (1), but calculations with these terms are not yet possible. The effects of the antisymmetrization of the projectile with the target nucleons have also been neglected. The knockout-exchange amplitudes have recently been

<sup>19</sup> We are grateful to A. D. Hill for making this program available to us.

<sup>20</sup> N. K. Glendenning and M. Veneroni, Phys. Rev. **144**, 839 (1966); G. R. Satchler, Nucl. Phys. **77**, 481 (1966).

shown to be large,<sup>21</sup> so that calculations of asymmetries with these terms included would be of considerable interest.

The microscopic-model predictions assumed a  $(\pi 1g_{9/2})_2^{+2}$  configuration for the 2.18-MeV state in  $^{90}\text{Zr}$  and a  $(\nu 2d_{5/2})_2^{+2}$  configuration for the 0.93-MeV state in  $^{92}\text{Zr}$ . The 1.51-MeV state in  $^{92}\text{Mo}$  is supposed to be a mixture of 82%  $(\pi 2p_{1/2})_0^{+2}(\pi 1g_{9/2})_2^{+2}$  and 18%  $(\pi 1g_{9/2})_2^{+4}$ , as suggested by Auerbach and Talmi.<sup>22</sup> Calculations of energy levels for the  $2^+$  and higher states of these configurations give good agreement with the data. The admixtures of other configurations, and especially of neutron configurations in  $^{90}\text{Zr}$ - $^{92}\text{Mo}$  and of proton configurations in  $^{92}\text{Zr}$ , are difficult to determine experimentally. However, the admixture of  $(\nu 2d_{5/2})_0^{+2}$  in the ground state of  $^{90}\text{Zr}$  is only about 2.5%, which indicates that  $N=50$  is quite a good closed shell.<sup>23</sup> Further, the  $(p, d)$  work of Ball and Fulmer<sup>23</sup> also indicates that the  $(\nu 1g_{9/2}^{-1} 2d_{5/2})_2^{+2}$  excitation lies at 4.22 MeV in  $^{90}\text{Zr}$ , and thus should not be expected to mix strongly with the 2.18-MeV level. In  $^{92}\text{Zr}$ , there is evidence<sup>15</sup> that the  $2^+$  state of the  $(\pi 1g_{9/2})_2^2$  configuration lies at 1.85 MeV, less than 1 MeV away from the 0.93-MeV  $(\nu 2d_{5/2})_2^{+2}$  state. Also, the spectroscopic factor<sup>24</sup> for excitation of the 0.93-MeV level in  $^{91}\text{Zr}(d, p)^{92}\text{Zr}$  exhausts only about 70% of the sum-rule limit. Thus, this state is probably less pure.

It is clear, of course, that these configurations are not pure, since the  $B(E2)$ 's determined from the electromagnetic transition rates are larger than the

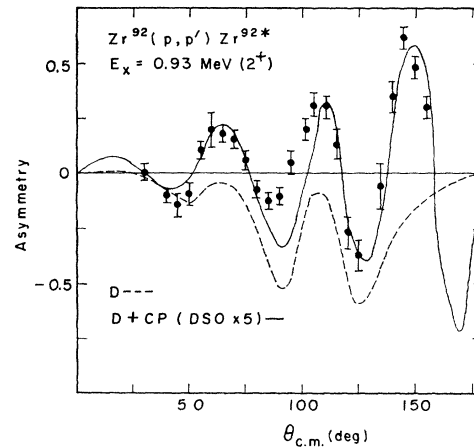


FIG. 9. Microscopic-model predictions for the 0.93-MeV state in  $^{92}\text{Zr}$ . The notation (DSO  $\times 5$ ) means that the strength of the DSO term was increased by a factor of 5 relative to the central terms in the CP form factor.

<sup>21</sup> D. Agassi and R. Schaeffer, Phys. Letters **26B**, 703 (1968); Jay Atkinson and V. A. Madsen, Phys. Rev. Letters **21**, 295 (1968).

<sup>22</sup> N. Auerbach and I. Talmi, Nucl. Phys. **64**, 458 (1965).

<sup>23</sup> J. B. Ball and C. B. Fulmer, Phys. Rev. **172**, 1199 (1968).

<sup>24</sup> B. L. Cohen and O. V. Chubinsky, Phys. Rev. **131**, 2184 (1963).

single-particle estimates. The effective charge has been found to be  $(2.4 \pm 0.5)e$  for the  $^{90}\text{Zr}$   $2^+$  transition and  $(1.83 \pm 0.15)e$  for  $^{92}\text{Zr}$ ,<sup>5</sup> the  $B(E2)$  for  $^{92}\text{Mo}$  is slightly larger than that for  $^{90}\text{Zr}$ .<sup>25</sup> To include these effects of core excitations in the microscopic description of inelastic scattering, Love and Satchler<sup>5</sup> use a form factor with two terms. The direct term arises from the simple configurations

$$I_L^{(1)}(r) = \int u_2(r_i) u_1(r_i) g_L(r, r_i) r_i^2 dr_i. \quad (2)$$

Here  $u_k(r_i)$  is the wave function of the valence particle bound in a Woods-Saxon well, and  $g_L(r, r_i)$  is the  $L$ th term in the multipole decomposition of  $g(|r_{ij}|)$  of Eq. (1). The second term arises from the assumed surface vibrations of the core

$$I_L^{(2)}(r) = (4\pi V_0)^{-1} y_L(Q) \langle n_2 l_2 j_2 | k_v | n_1 l_1 j_1 \rangle k_p(r_p), \quad (3)$$

where  $V_0$  is the strength of the direct interaction of Eq. (1), and where  $k_p(r_p)$ , which determines the shape of  $I_L^{(2)}$ , is proportional to the radial derivative of the optical potential. Thus,  $k_p$  contains a complex central term and a deformed spin-orbit term (DSO). The product  $y_L(Q) \langle k_v \rangle$  is a number which can be determined from the effective charge  $e_{\text{eff}}$ :

$$y_L(Q) \langle k_v \rangle = \frac{4\pi (e_{\text{eff}} - e_i) \langle n_2 l_2 j_2 | r_i^L | n_1 l_1 j_1 \rangle}{3Z_c e R_c^L}.$$

Here  $e_i$  is the charge on the valence particle,  $Z_c$  is the charge of the core, and  $R_c$  is the Coulomb radius. The matrix element  $\langle r_i^L \rangle$  is evaluated with the same Woods-Saxon wave functions used in Eq. (2). In the calculations which follow, all parameters are the same as those used by Love and Satchler,<sup>5</sup> with the exception of the optical parameters. The strength  $V_0$  was set to 80 MeV.

The predictions of the microscopic model for the asymmetry following excitation of the  $2^+$  state in  $^{90}\text{Zr}$  are shown in Fig. 8. It is clear that they are far from explaining the data. The predictions with only the direct term (D) for  $^{90}\text{Zr}$  are similar to the D predictions for  $^{54}\text{Fe}$  at 18.6 MeV<sup>1</sup> which were also unable to account for the large positive asymmetries. Unfortunately, the addition of core polarization does not improve the fit. In fact, if the deformation of the spin-orbit term is neglected [i.e., if the derivative of the spin-orbit term in the optical potential is not included in  $k_p$  in Eq. (3)], the fit is considerably worse.

Some predictions for  $^{92}\text{Zr}$  are shown in Fig. 9. The D curve is again in poor agreement with the data. It is interesting to note, however, that the oscillations in this curve have larger amplitudes than in the  $^{90}\text{Zr}$  D curve. The differences between the two curves arise partly from the differences in the form

<sup>25</sup> E. J. Martens and A. M. Bernstein, Nucl. Phys. A117, 241 (1968).

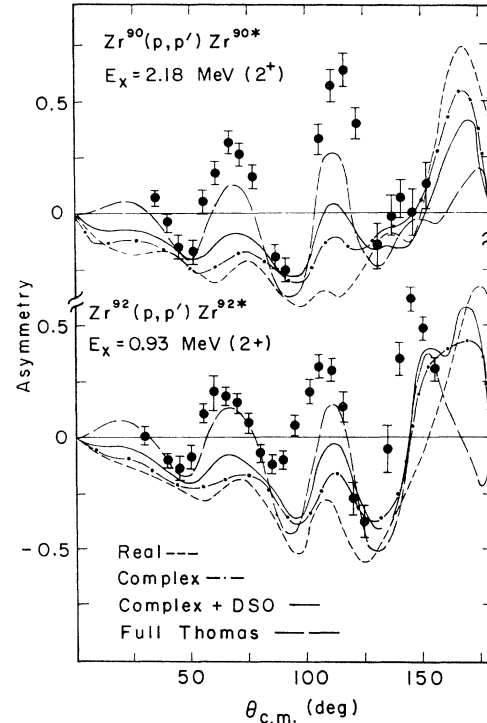


FIG. 10. Macroscopic-model predictions for the  $2^+$  states. In the calculations with the "Full-Thomas" term,  $\beta_{so}$  was set to  $1.5\beta(\text{central})$ .

factors and partly from the small differences in the optical parameters; both are significant. With the addition of CP, of normal strength, the predictions for  $^{92}\text{Zr}$  are again in worse agreement with the data; this curve is not shown. It is only by artificially increasing the strength of the deformed spin-orbit term in the CP part of the form factor that the reasonable agreement between theory and experiment shown by the solid curve in Fig. 9 is achieved. Even such extreme measures are not sufficient for  $^{90}\text{Zr}$ , chiefly because the magnitudes of the experimental asymmetries at the first two maxima are larger.

Fits to the data for  $^{92}\text{Mo}$  are not shown. The D predictions are very similar to the D predictions for  $^{90}\text{Zr}$ , since the form factors are assumed to be the same. Predictions for the cross sections in the microscopic model are also not illustrated, since very similar predictions have been shown before.<sup>5</sup> The fits are generally good, comparable to the best of those shown in Figs. 3-5. However, they are unable to match the difference in back-angle behavior between  $^{90}\text{Zr}$ - $^{92}\text{Mo}$  and  $^{92}\text{Zr}$ .

## 2. Macroscopic Model

For collective states the macroscopic model often provides an accurate description of both differential cross sections and asymmetries. Even for states for which the microscopic model would seem appropriate,

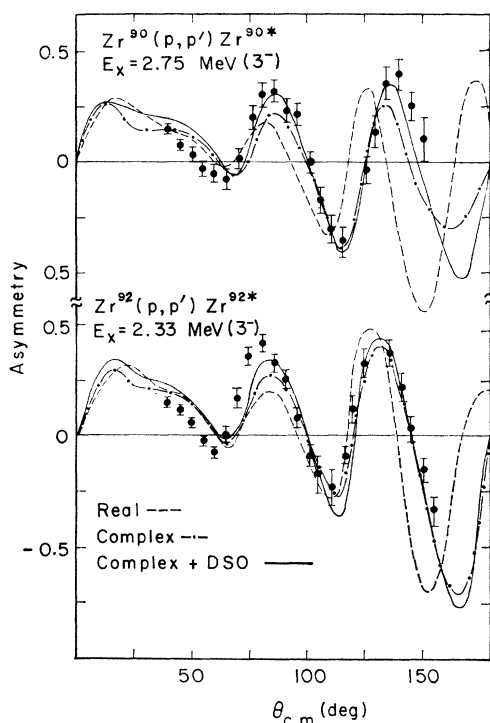


FIG. 11. Macroscopic-model predictions for the  $3^-$  states.

it often happens that the collective-model prediction is in better agreement with the data.

Predictions of this model, which has been described at length in the literature, are shown in Figs. 10 and 11. The various curves correspond to calculations with different form factors. The form factor is "Real" if only the real central term of the optical potential is deformed; it is "Complex" if both the real and imaginary central terms are deformed. The "Complex+DSO" calculations included the deformation of the entire optical potential<sup>1</sup>; the "Full Thomas" curves are described below. Coulomb excitation was included in the calculation of all these curves.

For the  $2^+$  asymmetries of Fig. 10, the addition of the imaginary and spin-orbit terms to the form factor each improves the fit, but the "Complex+DSO" prediction is still not better than the predictions of the microscopic model. The cross sections (Figs. 3-5) show a preference for real coupling only. (The "Complex+DSO" cross-section predictions are very similar to the "Complex" curves.) The agreement is then quite good for  $^{90}\text{Zr}$  and  $^{92}\text{Mo}$ , but the  $^{92}\text{Zr}$  cross sections are poorly fitted.

The collective-model predictions for the  $3^-$  asymmetries shown in Fig. 11 are considerably better. Again, the best fit is obtained with the entire optical potential deformed. Some problems remain at forward angles; the  $^{92}\text{Zr}$  asymmetry also is not well reproduced around  $70^\circ$ . The fits to the cross sections are also fairly good but it is necessary to note that real coupling again gives better agreement.

The deformed spin-orbit term which has been used thus far is proportional to the radial derivative of the spin-orbit term in the optical potential. Recently, Sherif and Blair<sup>26</sup> have shown that the fits to higher-energy asymmetry data could be improved, especially at forward angles, by including the derivatives of the angle-dependent terms as well. These terms arise if the "Full Thomas" expression for the spin-orbit potential is used, in analogy with the spin-orbit potential in atoms

$$U_{so} = (\hbar/m\pi c)^2 V_{so} \delta \cdot [\nabla(\rho(r)) \times i^{-1} \nabla],$$

where  $\rho(r)$  is the nuclear matter density. The introduction of this type of spin-orbit potential does not affect the elastic scattering analyses, since the targets have zero spin, but it does affect the inelastic scattering.

Calculations with the full Thomas term have been carried out by Sherif for the present data; they are illustrated in Figs. 10 and 12. In each case, the extra term brings a distinct improvement in the fit. The effect is most clear for the  $2^+$  where the increase in magnitude at the first maximum is almost sufficient to match the data for  $^{92}\text{Zr}$ . [The deformation parameter  $\beta_{so}$  for the spin-orbit term was set to  $1.5\beta$  (central) for this calculation.] The  $3^-$  fits are also considerably

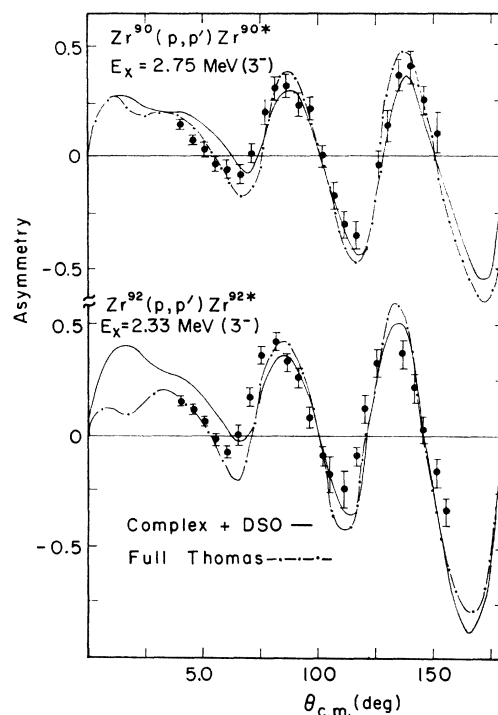


FIG. 12. The effect of the angle-dependent term in the "Full-Thomas" expression of the deformed spin-orbit potential. Both calculations are the same except for this term;  $\beta_{so}$  was set equal to  $\beta$  (central).

<sup>26</sup> H. Sherif and J. Blair, *Phys. Letters* **26B**, 489 (1968).

TABLE I. Best-fit optical-model parameters for 20.25-MeV protons.

Target	$V_s$ (MeV)	$r_s$ (F)	$a_s$ (F)	$W_D$ (MeV)	$r_T$ (F)	$a_T$ (F)	$V_{so}$ (MeV)	$r_{so}$ (F)	$a_{so}$ (F)	$\chi_\sigma^2$	$\chi_p^2$	$\chi^2/N$	$\sigma_R$
$^{90}\text{Zr}$	48.20	1.24	0.618	8.05	1.29	0.60	5.75	1.07	0.53	70	120	3.9	1240
$^{92}\text{Zr}$	47.82	1.26	0.609	9.32	1.30	0.57	6.30	1.14	0.53	93	186	5.9	1218
$^{92}\text{Mo}$	47.73	1.24	0.616	7.88	1.33	0.60	5.94	1.03	0.53	54	91	3.5	1221

better now at forward angles and not worse at larger angles; the over-all agreement is very good.

The effects of including an imaginary term in the spin-orbit potential were also explored. The predictions for the  $2^+$  state in  $^{54}\text{Fe}$  were found to be quite sensitive to such a term, but the elastic scattering was not well fitted when it was included. If an imaginary spin-orbit term of strength  $-1$  MeV was simply added to the potential of Table I, the predicted amplitudes of the asymmetries for the  $2^+$  state in  $^{92}\text{Zr}$  were greatly increased. Although the detailed shape was not well reproduced, the agreement in magnitude was good. However, when the other parameters were adjusted slightly to retain the fit to the elastic scattering, the effect of the imaginary spin-orbit term was much smaller.

## V. CONCLUSIONS

The results of this study of the asymmetry in the inelastic scattering of polarized protons from  $^{90}\text{Zr}$ ,  $^{92}\text{Zr}$ , and  $^{92}\text{Mo}$  are qualitatively similar to those reported earlier<sup>1</sup> for nuclei with  $A \sim 60$ . Interesting variations in the  $2^+$  cross sections and asymmetries were observed which microscopic-model calculations were unable to predict. On the other hand, good fits were obtained to the asymmetries for the collective states, in this case the  $3^-$  states, with a macroscopic model.

The addition of a core-polarization term to the microscopic form factor did not improve the agreement with the  $2^+$  asymmetry data, although it must be included to account for at least the magnitude of the differential cross sections. The effect of the CP term was investigated with two different optical potentials which gave very good fits to both the elastic cross-section and asymmetry data. It is possible that with some adjustment of these parameters better fits to the inelastic asymmetries could be found, but good

agreement is unlikely without large changes in the parameters. The disagreement should then be ascribed to the microscopic treatment itself. The effective force is real and it lacks tensor and spin-orbit terms. The fact that the deformations of both the imaginary and spin-orbit terms in the collective model increase the predicted asymmetries may be interpreted as evidence for similar terms in the effective interaction. However, a nucleon-nucleon spin-orbit force does not necessarily have the same effect as the deformed spin-orbit term. The neglect of the knockout-exchange amplitudes may also be important, although preliminary calculations by Schaeffer<sup>27</sup> indicate that the asymmetry predictions are not substantially improved when these amplitudes are included. Finally, the phenomenological treatment of the core polarization may not be sufficient for the analysis of asymmetry data.

In the macroscopic-model analysis, the fits obtained to the  $2^+$  data were equally poor unless the deformation of the full Thomas form of the spin-orbit potential was included. Even then the agreement was not satisfactory, but it might be improved with some small changes in the optical parameters. Collective-model predictions for the  $3^-$  asymmetry data were good except at forward angles without the full Thomas term. When this was included, the agreement at all angles was generally very good.

## ACKNOWLEDGMENTS

The authors gratefully acknowledge the indispensable help of R. Chaminade and the electronics groups, Mrs. A. Garin and her co-workers in the detector laboratory, and the entire cyclotron operating staff. We are indebted to Dr. A. G. Blair for his generous assistance in many phases of this work, and to Dr. P. Vaganov for his help in taking the data.

<sup>27</sup> R. Schaeffer (private communication).